*Tellus (1999), 51A, 412–430*
*Printed in UK – all rights reserved*


**TELLUS**
*ISSN 0280–6495*

# Parameterization of density-driven downsloping flow for a coarse-resolution ocean model in *z*-coordinate

By JEAN-MICHEL CAMPIN* and HUGUES GOOSSE, *Institut d'Astronomie et de Géophysique G. Lemaître, Université Catholique de Louvain, 2 Chemin du Cyclotron, B-1348 Louvain-la-Neuve, Belgium*

(Manuscript received 22 June 1998; in final form 2 February 1999)

ABSTRACT

In the World Ocean, densest waters found on the continental shelves induce density driven downsloping currents that can influence the deep ocean water masses properties. This process is poorly represented in *z*-coordinate ocean models, especially in Ocean General Circulation Model (OGCM) with coarse resolution in both horizontal and vertical directions. Consequently, continental shelves appear to be too isolated from the open ocean, whereas the density remains too low in the deep ocean. This study presents a simple parameterization of downsloping flow designed for *z*-coordinate, coarse resolution ocean model. At the shelf break, when the density on the shelf is higher than that in the neighbouring deep water column, a downsloping current is set up. This current is linearly related to the horizontal density gradient between the two adjacent boxes, using a prescribed coefficient. For simplicity, a uniform value of the coefficient is used here, although it should ideally vary in space. From the shelf, the downsloping flow is assumed to go downward along the slope until it reaches a level of equal density. An upward return flow of equal magnitude maintains the conservation of mass. This parameterization has been implemented in an OGCM and two experiments, with and without this scheme, have been integrated until equilibrium using restoring boundary conditions. The impact of the downsloping parameterization on the global ocean is dominated by the improvement of the Antarctic bottom water circulation and water mass properties. The parameterization increases the density of the deep ocean and tends to reduce the intensity and depth of the North Atlantic deep water circulation, which is in better agreement with observations. As a result of a higher exchange with the open ocean, the properties of continental shelf waters are also improved, with a marked reduction of the Antarctic shelves salinities. Therefore, this simple parameterization leads to a significant improvement of the model results, at little computational cost.

## 1. Introduction

Downsloping flow, associated with coastal dense water formation, is one of the two major sources of deep water for the World Ocean, the other being attributed to open ocean convection (Killworth, 1983). For instance, the Antarctic continental shelf water is very dense because of its low temperature and relatively high salinity. After mixing with warm circumpolar deep water, it can flow along the continental slope (Foster and Carmack, 1976; Baines and Condie, 1998), forming Antarctic bottom water (AABW) which feeds the deepest parts of the World Ocean. This has been confirmed by recent measurements indicating the existence of a continuous dense bottom layer along the continental slope in the Western Weddell Sea (Gordon et al., 1993; Muench and Gordon, 1995).

In the Arctic basin, it has been suggested (Swift et al., 1983; Aagaard et al., 1985) that the water in the deepest layer could be renewed through dense downsloping flow originating from the Arctic shelves. This is supported by observations,

* Corresponding author.
e-mail: campin@astr.ucl.ac.be

made near Svalbard (Schauer, 1995), of a downsloping plume dense enough to reach the deepest part of the Arctic or GIN Seas (Greenland, Iceland and Norwegian Seas). When the Arctic shelf water is not so dense, the downsloping flow is unable to reach the bottom. Then, according to its density, it joins intermediate levels (Schauer et al., 1997) or even subsurface levels and thus contributes to the salt budget of the Arctic halocline layer (Cavalieri and Martin, 1994; Steele et al., 1995).

In addition to shelf processes, downsloping flow plays a major rôle in the outflow of dense water from semi-enclosed seas through narrow passages, such as the Gibraltar Strait (Price et al., 1993) for the Mediterranean or the Faroe Bank Channel, Iceland Faroe Ridge, and Denmark Strait for the GIN Seas (Price and O'Neil Baringer, 1994). These waters flowing out of the Mediterranean and the GIN Seas largely determine the properties of North Atlantic intermediate water and North Atlantic deep water (NADW), respectively. Therefore, the downsloping outflow from the semi-enclosed seas can have an influence on the water characteristics at the global scale. There is also recent evidence (Polzin et al., 1996) that downsloping currents occurring through narrow gaps in the ocean ridges control the mixing of bottom water with overlying water.

Numerical models have been used to study downsloping currents in idealized cases (Smith, 1975; Killworth, 1977; Chapman and Gawarkiewicz, 1995; Shapiro and Hill, 1997) and in realistic regional applications (Price and O'Neil Baringer, 1994; Jungclaus et al., 1995). Nevertheless, until recently, this process was not properly represented in $z$-coordinate ocean general circulation models (OGCMs), despite its potentially large effect on deep water properties (Harvey, 1996). Two kinds of problems, outlined below, can explain this late interest: the first is related to the surface conditions triggering downsloping flow and the second is the inability of this kind of models to represent the process itself.

Downsloping fluxes depend crucially on the surface forcing, which, in many cases, is poorly represented. In shelf regions where downsloping flow occurs, the production of dense water is often intimately associated with sea-ice processes which are generally not taken explicitly into account. Sea-ice production is not uniformly distributed all over shelf regions but is mainly concentrated near the coast: in winter, when the winds tend to export sea-ice offshore, leaving the sea surface exposed to very cold continental air masses, ice formation can be very intense (Gill, 1973). This, through both large heat loss and brine rejection, increases the surface water density (Zwally et al., 1985; Fahrbach et al., 1994). In OGCMs which do not explicitly include sea-ice, this complex salinity flux distribution is represented by prescribed fluxes from field data or replaced by a restoring term toward observed salinity. But, since winter observations are scarce and sea-ice production is highly concentrated (both in time and space), the climatological mean over one OGCM mesh cannot reflect the corresponding density maximum. To cope with this problem, it has been proposed to increase the restoring salinity near Antarctica (salt adjustment) (England, 1993; Hirst and Cai, 1994). However, for the above reason, the amplitude and geographical distribution of salt adjustments cannot be objectively determined by quantitative observations all over Antarctica and thus remain somewhat arbitrary. Consequently, it appears difficult to clearly assess the effect of a missing process such as downsloping flow, since it can be hidden by too strong a salt enhancement. In particular, Toggweiler and Samuels (1995) discussed the effect of salt adjustment around antarctica: using a "realistic" salinity enhancement limited to the shelf (experiment "500 m restored"), the shelf salinity increased significantly ($+0.4$ psu), but only a small impact ($+0.02$ psu) was noticed on the properties of the deep ocean which remained too fresh ($-0.15$ psu) compared to observations. These authors concluded that this fresh bias was not due to unrealistic surface salt flux on the Antarctic shelf but was related to other model deficiencies. Here, it is suggested that the inappropriate representation of downsloping processes should also play a rôle in the results of Toggweiler and Samuels (1995).

Even in the OGCMs which include a comprehensive sea-ice component, the coarseness of the grid and the fact that the surface forcing lacks extreme meteorological events such as katabatic winds (Gallée, 1995) imply that the intense sea-ice production and the associated surface dense water formation occurring in narrow coastal regions are not properly represented. Nevertheless,

at medium or large scales, such models are able to provide a correct order of magnitude of sea-ice production (Goosse et al., 1997a).

The second reason why downsloping flows are not properly taken into account in OGCMs lies in the characteristics of the numerical grid used, i.e., the coarseness of the resolution and the use of the vertical "$z$-coordinate". In particular, the latter, by transforming the ocean bottom into a kind of staircase, renders it difficult to represent realistically small-scale phenomena that crucially depend on the details of the bottom topography. Recently, attempts have been made to include an explicit representation of the bottom boundary layer in $z$-coordinate OGCMs (Gnanadesikan et al., 1998; Killworth and Edwords, 1998). Those new schemes will undoubtedly improve models results since they imply an increase in vertical resolution near the bottom, offering thereby the opportunity to distinguish the dynamics of the bottom boundary layer from that of the overlying ocean. However, this increases the model complexity, leading to extra computational cost. Furthermore, small-scale bathymetric features that play an important rôle in downsloping processes (Baines and Condie, 1998), cannot be represented in a coarse horizontal resolution model, even with a bottom layer formulation.

Herein, an alternative, simpler approach is suggested, consisting in parameterizing the effect of downsloping flows without resolving the bottom boundary layer. This new method, which is well-suited for coarse resolution $z$-coordinate models, is described in Section 2. The differences with the recently-published parameterization of Beckmann and Döscher (1997), developed for similar purposes, are highlighted.

In general, idealized test cases cannot account for the variety of bottom shapes and density structures found in the World Ocean. Therefore, we directly address the effects of the new parameterization in an OGCM using a realistic representation of the bathymetry and the forcing (Section 3). For this purpose, two experiments, with and without the downsloping parameterization, have been integrated until equilibrium, under annual mean forcing with moderate salt enhancement over the Antarctic continental shelves. The results thereof are analyzed in Section 4. Finally, conclusions are drawn in Section 5.

## 2. Description of the downsloping parameterization

The purpose of the downsloping parameterization proposed here is to represent the effect of density-driven downsloping flow, rather than the flow itself. It is intended for a $z$-coordinate, coarse horizontal resolution model, i.e., for most OGCMs. An important aspect of this parameterization comes from the scale ratio between the model resolution ($3^\circ \times 3^\circ$ in this study) and the real size of downsloping process. Concerning the space scale, a thickness of 100 m seems realistic for a fully developed plume (Killworth, 1977) and a rough estimate of the horizontal layer width in the slope direction, of the order of 10 km, can be derived from observations (Muench and Gordon, 1995; Schauer, 1995; Schauer et al., 1997). Since this layer is far too small to be represented in a coarse resolution model, the parameterization simply ignores it. For the same reason, the parameterization has no direct action on the resolved velocity field and only modifies the model scalar quantities, such as the potential temperature $\theta$ (°C), the salinity $S$ (psu) and any additional tracer. The phenomena which we intend to account for may be described as follows.

(1) Downsloping flow occurs when density above the sea floor, at the top of the slope, is larger than the surrounding water in the deeper ocean. The density difference causes dense water to move down the slope. For simplicity, the starting point of the downsloping flow will be referred to as the shelf break; but of course, downsloping flow may occur in many other bathymetric configurations.

(2) Intense mixing occurs at the beginning of the downward stream, at the shelf break and just below it. The mixing is a consequence of relatively large entrainment of ambient water and depends of the speed of the downsloping current (Price and O'Neil Baringer, 1994); in the presence of canyons, this mixing effect is smaller (Chapman and Gawarkiewicz, 1995). Below this high-entrainment region, mixing is strongly reduced. This is supported by the presence of a well defined, very thin cold layer that is stuck to the continental slope, as shown in Fig. 5 of Muench and Gordon (1995).

(3) The downsloping flow moves downward until it encounters a water level of equal density,

then splits and merges into the ambient water. Otherwise, if it is denser than any water in the deep ocean, it fills the bottom layer.

Our parameterization is designed in accordance with the above description.

The downsloping scheme is activated if the density $\rho^{sh}_{kup}$ of a grid box $B^{sh}_{kup}$ at the top of a bathymetric step (Fig. 1) is greater than $\rho^{do}_{kup}$ in the neighbouring box $B^{do}_{kup}$ located at the same level, in the region where the ocean is deeper.

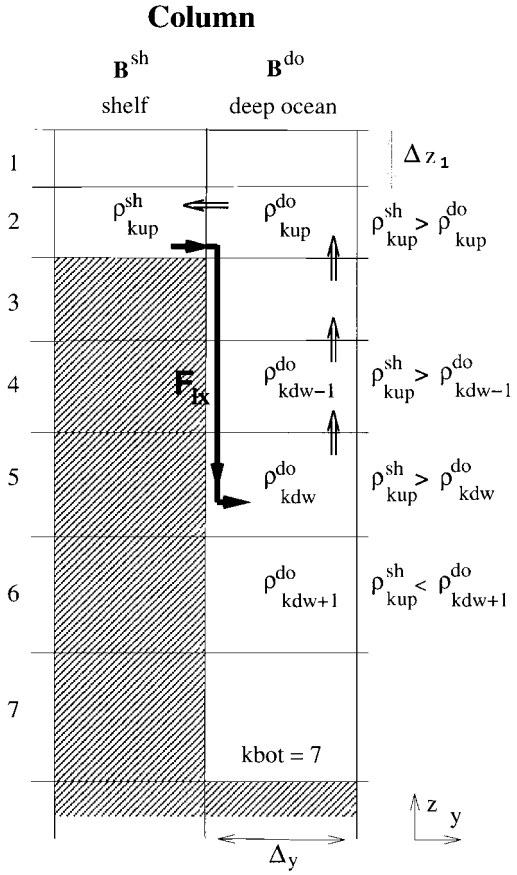


*Fig. 1.* The downsloping parameterization scheme is represented in the $Y$–$Z$ plane. The dense water ($\rho^{sh}_{kup}$) in the bottom level ($B^{sh}_{kup}$, $kup = 2$) of the shallow water column ($B^{sh}$) generates a downsloping flow ($Flx$) (simple thick arrow) function of the density difference $\Delta\rho = \rho^{sh}_{kup} - \rho^{do}_{kup}$; it joins the grid box $B^{do}_{kdw}$ in the deeper ocean water column ($B^{do}$) at the level of equal density (see the text) $kdw = 5$. Also drawn is the upward/horizontal return flow (double thin arrows) that involves the same volume transport ($Flx$).

Since the real downsloping flow is generally not directly correlated with the direction and intensity of the large scale current, especially in the case of complex bottom shape, it can hardly be evaluated from the velocity given by the standard model (hereafter referred to as the "original current") between $B^{sh}_{kup}$ and $B^{do}_{kup}$. On the contrary, the expression of the transport ($Flx$) induced by the downsloping flow must directly take into account the density difference $\Delta\rho = \rho^{sh}_{kup} - \rho^{do}_{kup}$. This requires a specific relation for the transport ($Flx$), that must however remain simple, because a comprehensive representation would require local parameters that cannot be estimated in our case.

For these reasons, the downsloping velocity ($v'$) is evaluated from a simple equilibrium between the driving force, assumed proportional to $\Delta\rho$ and a drag force proportional to $v'$:

$$0 = \frac{g}{\rho_0}\ \alpha\,\Delta\rho - \mu v', \tag{1}$$

where $\alpha$, $g$ and $\rho_0$ represent the slope, the gravity acceleration and the reference density and $\mu$ is a measure of the processes that inhibit the descent of the plume. This relation is similar to the "simplest momentum balance" derived by Chapman and Gawarkiewicz (1995) (their eq. (15) and Fig. 15) for a canyon downsloping plume.

Then, the transport ($Flx$) of the downsloping flow, here in the $Y$ direction (Fig. 1), is simply given by the product of the speed ($v'$) of the descending plume and the cross section surface ($\Sigma$) involved in the downsloping flow. Since only a part of the real edge section is able to initiate a downsloping flow in the $Y$ direction, the surface $\Sigma$ is taken as a fraction $\delta$ ($0 < \delta < 1$) of the mesh size, leading subsequently to the linear relation:

$$Flx = \gamma g \frac{\Delta\rho}{\rho_0}\,\Delta x\,\Delta z_{kup} \tag{2}$$

with the coefficient of proportionality $\gamma = \delta\alpha/\mu$; $\Delta x$ and $\Delta z_k$ are the grid spacing in the $X$ and $Z$ directions.

This flow is supposed to go down the slope and to reach the level of equal density, $kdw$, defined as:

$$\rho(\theta^{sh}_{kup}, S^{sh}_{kup}, z_{kdw}) = \rho^{sh}_{kdw} \geqslant \rho^{do}_{kdw} = \rho(\theta^{do}_{kdw}, S^{do}_{kdw}, z_{kdw}),$$

$$\rho(\theta^{sh}_{kup}, S^{sh}_{kup}, z_{kdw+1}) = \rho^{sh}_{kdw+1} < \rho^{do}_{kdw+1} = \rho(\theta^{do}_{kdw+1}, S^{do}_{kdw+1}, z_{kdw+1}),$$

leading to a net transport from $B^{sh}_{kup}$ to $B^{do}_{kdw}$. If the density in all grid boxes of the water column $B^{do}$ is lighter than the density of the water coming from the shelf ($B^{sh}_{kup}$) evaluated at the right depth, the downsloping flow reaches the bottom ($kdw = k\text{bot}$). In order to ensure the volume conservation for the two boxes $B^{sh}_{kup}$ and $B^{do}_{kdw}$, an upward return flow is assumed from $B^{do}_{kdw}$ to $B^{do}_{kdw-1}$ until $B^{do}_{kup}$ and then horizontally from $B^{do}_{kup}$ to $B^{sh}_{kup}$. Even if the real pathway is probably more complex, this pattern seems more logical than a direct return flow from $B^{do}_{kdw}$ to $B^{sh}_{kup}$ since, in the real ocean, deep water properties at the level $kdw$ do not influence directly the top of the step ($B^{sh}_{kup}$).

The scalar properties are advected by this additional transport $Flx$ using the upwind scheme. For example, at the time step $n+1$, the salinities $S^{sh}_{kup}(n+1)$, $(S^{do}_{k}(n+1),\ k = kup, \ldots, kdw)$ of the corresponding boxes $B^{sh}_{kup}$, $B^{do}_{k}$ are modified by the downsloping flow (3a), the horizontal (3b) and the upward (3c) return flows as follows:

$$S^{do}_{kdw}(n+1) = \tilde{S}^{do}_{kdw}(n+1) + \frac{\Delta t_{kdw}}{\Delta x\, \Delta y\, \Delta z_{kdw}} Flx \times (S^{sh}_{kup}(n) - S^{do}_{kdw}(n)), \quad (3a)$$

$$S^{sh}_{kup}(n+1) = \tilde{S}^{sh}_{kup}(n+1) + \frac{\Delta t_{kup}}{\Delta x\, \Delta y\, \Delta z_{kup}} Flx \times (S^{do}_{kup}(n) - S^{sh}_{kup}(n)), \quad (3b)$$

and for $k = kdw - 1, \ldots, kup$:

$$S^{do}_{k}(n+1) = \tilde{S}^{do}_{k}(n+1) + \frac{\Delta t_{k}}{\Delta x\, \Delta y\, \Delta z_{k}} Flx \times (S^{do}_{k+1}(n) - S^{do}_{k}(n)), \quad (3c)$$

where $\tilde{S}_k(n+1)$ represents the updated salinity according to the original standard model (Section 7), $\Delta x, \Delta y, \Delta z_k$ the grid spacing in the three directions, and $\Delta t_k$ is the time step that can depend of the level $k$ if the convergence accelerator of Bryan and Lewis (1979) is applied. The parameterization assumes that downsloping flow develops during a characteristic time much longer than the time step, which is clearly the case in our simulation. Note that this scheme preserves the stability of the column $B^{do}$ if the non-linear effects of the equation of state are not dominant.

The downsloping parameterization is implemented in a simple way. The location of each bathymetric step is computed before the integration starts and stored in a specific list. At each time step, the list of potential downsloping flow is checked and, in the case of a positive density difference ($\rho^{sh}_{kup} > \rho^{do}_{kup}$), the downsloping routine is activated. Thanks to the simplicity of the parameterization, the computer time spent in this routine is negligible (about 1% of the total).

The main assumptions are presented below.

Concerning the parameter $\gamma$, the coefficients $\alpha$, $\mu$ and $\delta$ should vary from place to place implying a different value of $\gamma$ for each bathymetric step. But, for simplicity, and because no direct estimation of this parameter is available, a uniform value has been retained in our simulations. Parameter $\gamma$ should also depend on the depth, especially if the vertical resolution is not uniform. However, a compensation occurs for the latter problem. When the vertical grid size exceeds the thickness of the real downsloping flow, the surface $\Sigma$, tends to be overestimated. On the other hand, the density difference $\Delta\rho$ underestimates the real density contrast between the plume and the ambient water, because of an internal dilution effect in a grid box thicker than the plume. In this case, it can be shown with simple linear assumptions, that those two tendencies balance each other so that the relation (2) remains unchanged.

To give an idea of the range of possibles values for the parameter $\gamma$, we refer again to eq. (1) from the idealized canyon plume regime of Chapman and Gawarkiewicz (1995) (their Fig. 15). Taking their value of the coefficient $\mu = 10^{-4}\,s^{-1}$ and a rough estimate of the slope $\alpha \sim 3 \cdot 10^{-3}$, of the order of the Antarctic continental shelf slope, yields $\gamma = \delta\alpha/\mu \sim \delta \times 30$ s. As only the part $\delta$ of the mesh is concerned by the downsloping currents, a range for the parameter $\gamma$ between 1 and 10 s appears reasonable. The upper bound value $\gamma = 10$ s has been retained for the downsloping experiment in order to maximize the effects of the parameterization in this sensitivity test.

The parameterization does not refer explicitly to the Coriolis factor. Nevertheless, at large scale, the Coriolis effect is taken into account since the downsloping parameterization modifies the density field; this induces an adjustment of the current simulated by the model according to the geostrophic balance. Even at small scale, the tendency of the Coriolis effect to reduce the downward

movement of the plume can be included in the parameter $\gamma$.

The problem of mixing also needs to be discussed. In the observations, the mixing is intense at the shelf break. This is represented, to some extent, by the return flow from $B^{do}_{kup}$ to $B^{sh}_{kup}$ (Fig. 1) implying an internal mixing in the box $B^{sh}_{kup}$. Furthermore, the horizontal extent of the downsloping flow is usually much smaller than the grid size, so that merging into a grid box where a single average scalar property is defined is equivalent to a relatively large mixing. We believe that this internal mixing on the step, probably too large in some cases, can partly compensate for the lack of mixing below, at intermediate depths (levels $k$, from $kup+1$ to $kdw-1$). Nevertheless, in the real ocean, this mixing at intermediate depths is probably not very large, since the flow tends to maintain its main characteristics especially when canyons or ridges limit the development of eddies (Chapman and Gawarkiewicz, 1995) and reduce the mixing effect. Furthermore, this remark related to the lack of mixing in the model, at intermediate depths, only concerns the steep slope represented by a vertical wall in a coarse resolution model; otherwise, a stair like model bathymetry, corresponding to a smooth slope, allows the downsloping flow to cascade from one step to the other, implying an internal mixing at each intermediate level.

Another method to take into account downsloping flow in OGCM has been proposed by Beckmann and Döscher (1997) (hereafter referred to as B&D). Here we will discuss the main theoretical differences between the two schemes, since the comparison of the effect in an OGCM is not yet available. The idea of B&D is to take advantage of the $\sigma$ coordinate in the representation of bottom currents such as downsloping currents. Thus, they introduced locally, near a step, a part of $\sigma$ coordinate advection scheme into the usual $z$-coordinate discretization. In their scheme, the large scale flow calculated by the original standard model is directly used to deduce the up/downslope transport term. Only the path of the flow is changed.

One of the major differences with our parameterization is that the B&D scheme allows both downsloping and upsloping flow, depending of the direction of the original current between $B^{sh}_{kup}$ and $B^{do}_{kup}$. Consequently, their scheme can lead to an upsloping of denser bottom water to the shelf or a downsloping flow of lighter water. In our parameterization, an exchange of water is prescribed only in the case of density driven downsloping flow, and nothing is done in the three others cases. Furthermore, when the B&D scheme prescribes a downsloping flow, it is always incorporated into the bottom level $B^{do}_{kbot}$ irrespective of the densities on the shelf and in the deep ocean. On the contrary, our parameterization determines the inflow level $B^{do}_{kdw}$ according to the density structure of the deep ocean water column $B^{do}$ relative to the shelf ($B^{sh}_{kup}$).

Our intention is not to decide which scheme is better, but only to point out the differences. In a medium resolution model, the B&D scheme will probably provide a large improvement, as they showed in an idealized test case. In this experiment, the presence of many steps along the slope makes it possible to represent the downsloping flow at each level. With such a resolution, our parameterization would have a similar effect. The comparison of the results of both parameterization will not be convincing since here we introduced one additional parameter ($\gamma$) which could be easely tuned. On the other hand, in a coarse resolution model as ours, a steep slope is represented by a vertical wall, as, for example, the Barents Sea shelf break. In this case, the B&D scheme will tend to advect shelf water directly to the bottom of the Arctic Ocean and will not offer the opportunity to feed the Arctic halocline neither to reach an intermediate depth as observed (Schauer et al., 1997). Note that in a case of very steep shelf break, the $\sigma$ coordinate is not believed to be the most appropriate approach (Haney, 1991). Concerning the Barents Sea shelf break, the same remark can be applied to the more complex bottom boundary layer scheme of Gnanadesikan et al. (1998) or Killworth and Edwards (1998). But because those 2 schemes are very different and much more complex than our parameterization, a comparison cannot be easily drawn up on a theoretical base, but instead requires numerical tests results.

## 3. Numerical experiments design

The OGCM used to test this parameterization has been developed at the Université Catholique de Louvain (Deleersnijder and Campin, 1995;

Deleersnijder et al., 1997; Campin, 1997) and is the oceanic part of the coupled large-scale ice–ocean model "CLIO" (Goosse et al., 1997a,b,c). Details concerning the ocean model are given in Section 7.

In this preliminary study, a simple climatological annual mean forcing is used. The annual mean wind stress of Han and Lee (1983) is applied and sea surface temperature (SST) and salinity (SSS) are restored (restoring time $\tau = 7.5$ days) toward the annual mean climatology (Levitus, 1982). Despite the fact that restoring is not physically justified, especially for salinity, this kind of forcing enables us to keep the surface temperature and salinity close to the observations and can be also considered as a simple nudging technique. Another advantage is that the sea surface properties (SST, SSS) are better known than climatological fluxes that contain large uncertainties, especially in high latitudes (da Silva et al., 1994).

Because deep water is mainly formed in winter, when surface density reaches its maximum, the restoring temperatures north of 65°N have been shifted toward winter values, following the approach proposed by Hirst and Cai (1994). Furthermore, the salinity is enhanced ( + 0.4 psu) on the Antarctic continental shelves. This salinity adjustment is used to crudely represent the effect of ice production on the shelf (see Section 1). In fact, the only two regions concerned by this salt correction are the shallowest part ($H < 500$ m) of the Ross and Weddell Seas, with a salinity maximum that reaches respectively 35.00 psu and 34.85 psu. These values lie in the upper bounds of salinity measurements on those shelves (Jacobs et al., 1970; Foldvik et al., 1985). As proposed by Hirst and Cai (1994), SST and SSS of two grid boxes overmapping the Golfe du Lion in the Mediterranean have been modified toward winter values and a weak restoring ($\tau = 1$ year) toward observed temperatures and salinities (Levitus, 1982) is applied at 500 m in the gulf of Aden to simulate the Red Sea outflow, absent of the model domain. Note that, contrary to Antarctic shelves, no salinity enhancement is imposed in the Arctic region, since applying a strong salinity correction there, permanently and, at least, over one grid cell seems not justified regarding the characteristics of brine release in those regions (Cavalieri and Martin, 1994).

## 4. Results

The impact of the parameterization is analyzed through two experiments. In the first one (DWS), the downsloping flow parameterization is included but not in the second one (CTR). For both experiments, the model has been integrated until the equilibrium for several thousand years (1.7 *k*yr at the surface, 5.4 *k*yr at the deepest level). The direct effects, near regions where downsloping flows are active, are presented first and the remote large scale effects follow.

### 4.1. *Local effects*

The number of downsloping events is quite large ($\simeq 1.100$ points compared to $\simeq 3.100$ bathymetric steps), but many of them correspond to small exchange, especially in the deep ocean where the number of potential sites is large but the density differences are often small. In the deepest part of the ocean model, the coarse resolution $z$-coordinate model and the crude representation of the bathymetry that follows, do not allow an easy correspondence between simulated and few observed downsloping flows (Polzin et al., 1996). Nevertheless, the effect of the parameterization seems realistic and increases the density and the stratification of the deepest levels. For example, at the deepest level interface (4.8 km), the mean square of the Brunt–Väisälä frequency increases by 70% from $5.3 \cdot 10^{-8}$ in CTR to $9.1 \cdot 10^{-8}\,s^{-2}$ in DWS. The parameterization improves also the deepest level temperature and salinity since the average absolute differences with Levitus (1982) data is reduced respectively from 0.536°C and 0.0449 psu in CTR to 0.256°C and 0.0302 psu in DWS.

The large downsloping flows associated with high density differences are found mainly at high latitudes and correspond to sills or shelf break regions. The maximum downsloping flow (4.2 Sv, $1\ Sv = 10^6\ m^3/s$) is southward, located in the Western part of the Denmark Strait (Fig. 2), and follows the bottom from 1240 m to 1780 m. This transport is larger than current estimation of the total Denmark Strait Outflow (2.9 Sv, Dickson and Brown, 1994) for several possible reasons. First, the level thickness (420 m) is larger than the real dense water layer so that the model downsloping flow already incorporates a part of ambient

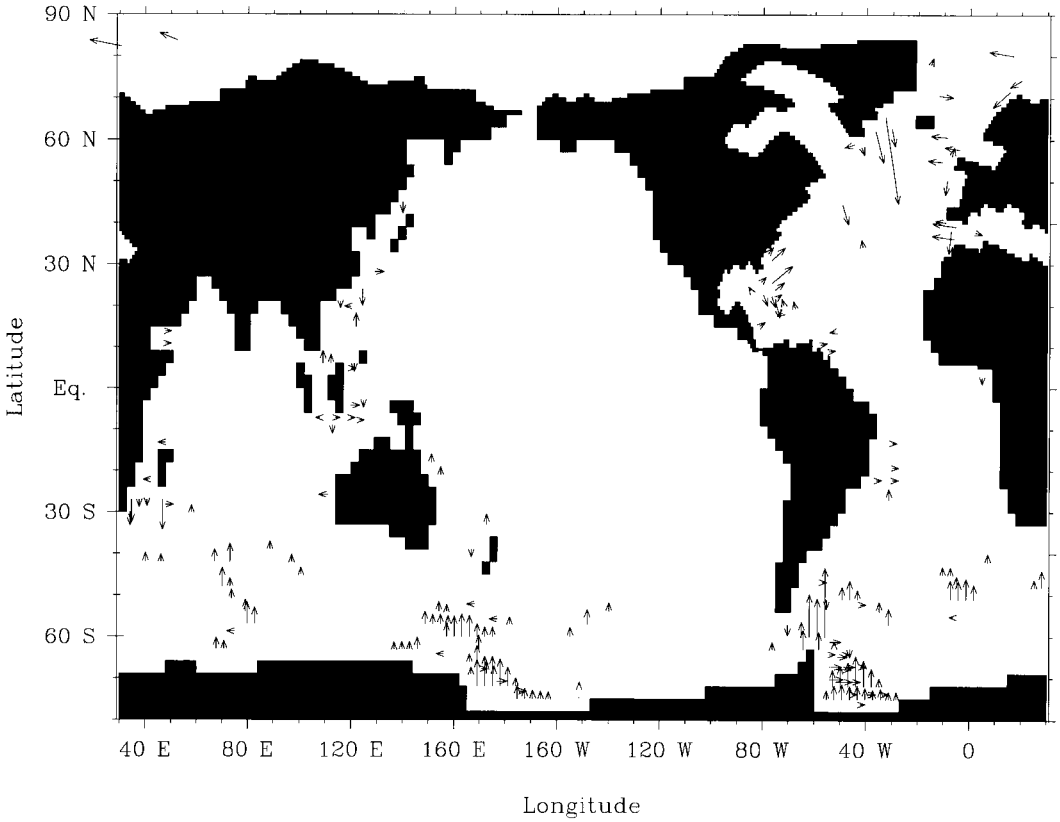


*Fig. 2.* Simulated downsloping transports (Sv) represented by arrows. Values below 1.6 Sv have not been drawn. The largest transport is found in the Denmark Strait and reaches 4.2 Sv.

water into it, leading to a larger estimation. Furthermore, the model simulates no southward flow through the Iceland–Scotland Strait and the Denmark Strait concentrates the total outflow from the GIN Seas (estimation: 5.6 Sv, Dickson and Brown, 1994). Finally, the deepening of the Denmark Strait ($H_{\text{sill}} = 1400$ m, but less than 900 m in the reality) makes the direct comparison difficult. This downsloping flow is associated with a significant northward heat transport (0.038 PW), but a much more reduced salinity exchange, because the Denmark Strait Outflow Water (DSOW) is colder than surrounding water ($\Delta\theta = -2.3°\text{C}$) but only slightly fresher ($\Delta S = -3.7 \cdot 10^{-2}$ psu).

In the high latitudes of the real ocean, because of heat loss and salt release during sea-ice formation, the dense water of shelf regions induces frequently downsloping currents, as mentioned above. However, Arctic shelves are not the best example of the parameterization effect because the forcing used is unable to reproduce the extreme events which induce dense water formation (Section 3). As a consequence, Arctic shelf waters remain too fresh in the model and thus not dense enough to generate downsloping flow. The only exception is the Barents Sea where the inflow of relatively warm and salty Atlantic water is modified through large surface heat loss and becomes dense enough to initiate a weak downsloping flow toward the deep Arctic Ocean.

On the Antarctic continental shelves, the salinity increase due to sea-ice formation is taken into account in the model, via a restoring to the enhanced SSS (Section 3) from Levitus (1982). This allows the production of high density shelf water that can downslope from the shelves to reach the deep ocean (Figs. 2, 3b). In the central

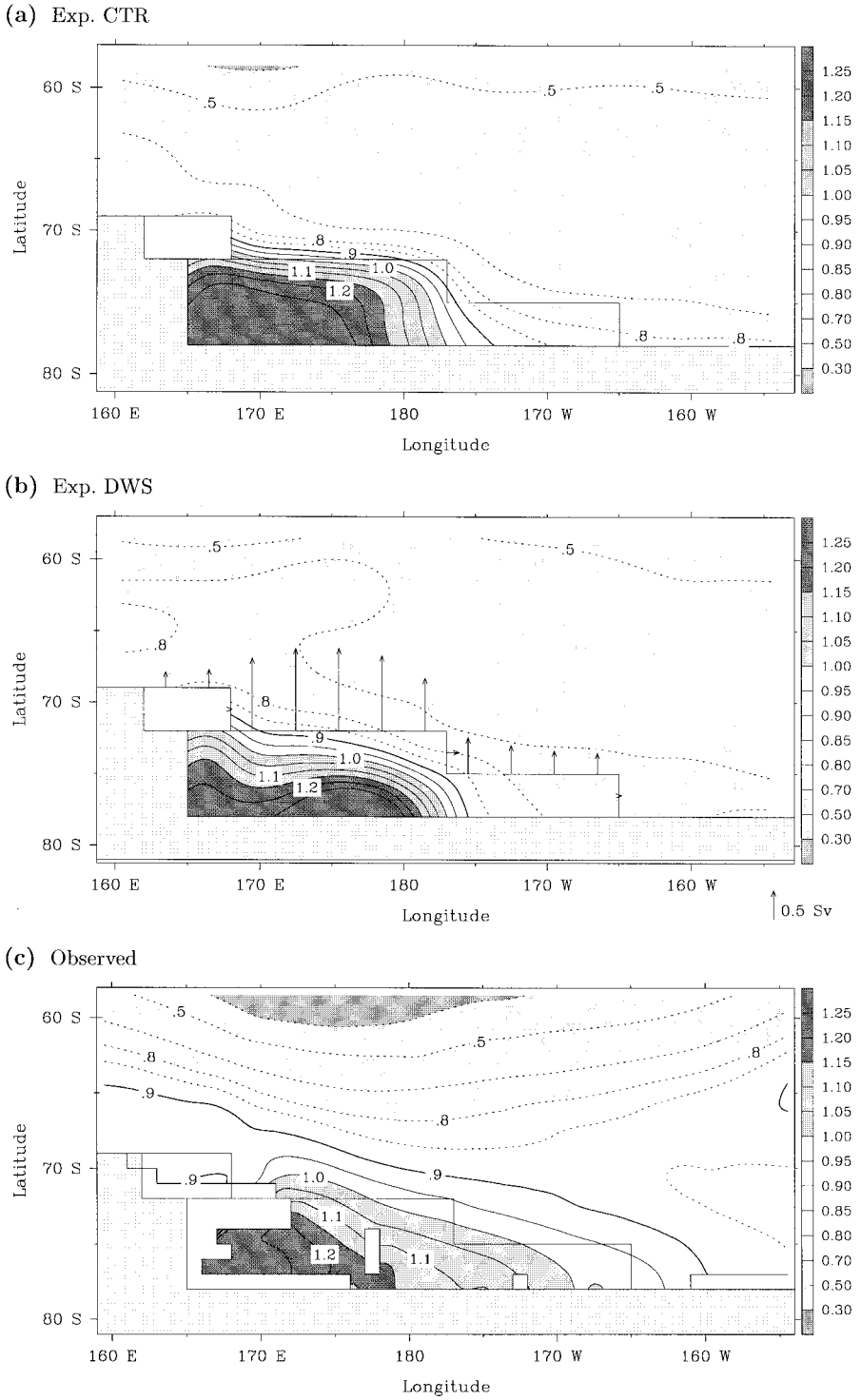


*Fig. 3.* Density (kg/m$^3$) relative to a reference water mass (4°C, 34 psu) at the bottom level (520 m) of the Ross Sea continental shelf, for (a) experiment CTR, (b) experiment DWS and (c) from Levitus (1982). The downsloping transport (in Sv) is represented by arrows in (b) (see the scaling, 0.5 Sv, on the right bottom corner). A thin black line marks the shelf edge position.

and Western part of the Ross and Weddell Sea continental shelves, the very dense shelf water induces large downsloping flows mainly toward the North and, to a smaller extent, toward the East. This water is dense enough to reach the local bottom level, with a falling height around 2000 m or more. This downsloping current can even initiate a second deeper cascading downsloping flow, as in the deep Weddell Sea (Fig. 2). By contrast, in the far Eastern part of the Weddell Sea and in the whole East Ross Sea, downsloping flows are less intense than in the Western part, and can only reach intermediate depths. This contrast comes from the cyclonic horizontal circulation in those regions. The supply of light water onto the Eastern part of those shelves partly balances the surface forcing densification effect and decreases the density contrast with open ocean, implying weaker and shallower downsloping flows than in the Western part.

In the model, the total downsloping flow that escapes the Antarctic continental shelf is large. For example, for the Weddell Sea continental shelf, the total outflow reaches 8.2 Sv, larger than current estimations: Muench and Gordon (1995) evaluate the northward transport of the bottom layer in the deep Western Weddell Sea to about 5 to 6 Sv, but this estimation already includes entrainment and mixing with open ocean water. However, the direct comparison with observations is not so easy, for the reasons that follow. First, part of the downsloping flows joins intermediate levels (e.g., in the Ross Sea, 27% of the total downsloping transport (8.6 Sv) from the shelf remains confined to the upper 1 km) and should be excluded from the shelf bottom water outflow budget when comparison is made with observations. Secondly, the thickness of the bottom shelf level (240 m at the depth of 520 m) is larger than the thickness of any downsloping plume, leading to an overestimation of the flow. A third point is that the high value of the parameter $\gamma$ retained in this simulation, in the upper range of the current estimation (Section 2), could be too large. The fourth reason comes from the crude representation, in the model, of the fine structure of the real forcing. The highest density shelf water are formed through small scale processes (e.g., related to Ice Shelves or coastal polynyas) or during short events (e.g., cold winter storm) that are not represented in the model, especially with an annual mean forcing. Therefore, to give the model a chance to reach the local density maximum, the extreme conditions have to be applied permanently and over at least one grid box. This may contribute to a larger surface buoyancy flux and consequently to a larger outflow than observed.

The parameterization effect can be noticed on the ocean density structure near Antarctic shelves, in the Ross and Weddell Seas (Figs. 3, 4, respectively), both reflecting higher exchanges with the open ocean. Without the parameterization, the dense water tends to be trapped on the shelf, resulting in a sharp density contrast with the open ocean. The downsloping flow allows this dense water to escape more easily from the shelf and replaces it by lighter open ocean water. The density patterns are then smoothed and become closer to the observations (Figs. 3, 4) compared to the control experiment (CTR).

### 4.2. *Global effects*

At the global scale, the density of AABW increases in DWS as a consequence of a larger exchange of Antarctic Shelf Water with the deep ocean. This appears clearly on the horizontally-averaged vertical density profile (Fig. 5) with higher density below 1.5 km compared to the CTR experiment. The density becomes closer to the Levitus (1982) profile, slightly too high between 1.8 and 2.5 km, and hardly distinguishable from observations below 2.5 km, whereas the density in the control experiment is too low in the deep ocean. This parameterization has no significant impact on intermediate water, which remains too warm and then too light compared to Levitus (1982) climatology (Fig. 5). Also noticeable, the positive density difference between the two simulations (DWS–CTR) (Figs. 5, 6a) increases gradually with depth and leads to a stronger stratification of the deep ocean in DWS. This density difference appears almost homogeneous in the meridional direction (Fig. 6a), except south of 50°S, between 0.5 km and 4 km where it is stronger. This can explain the strengthening of the ACC (from 120 Sv to 134 Sv) since the densification of the Weddell Sea Water column is responsible for a stronger meridional pressure gradient across the Drake passage (Cai and Baines, 1996). But, except the intensification of the ACC, the barotropic circula-

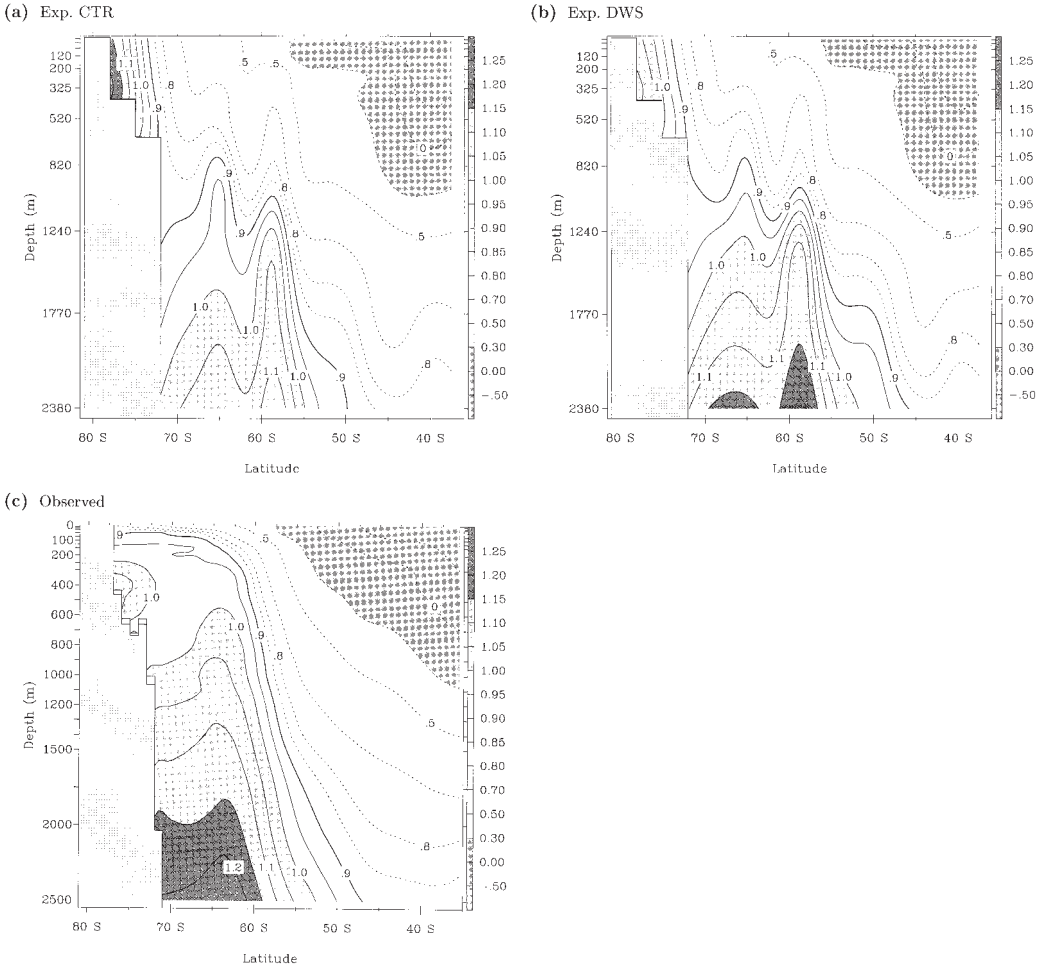


*Fig. 4.* Density structure in the meridional section at 50°W, across the Weddell Sea, for (a) experiment CTR, (b) experiment DWS and (c) from Levitus (1982). In order to remove the pressure effect, density differences ($kg/m^3$) relative to a reference water mass (4°C, 34 psu) are represented.

tion (not shown) remains roughly unchanged in both experiments.

This increase of AABW density has a significant impact on the thermohaline circulation, since the balance between the too main deep water masses, NADW and AABW, is better represented in the DWS experiment. In the Atlantic (Fig. 7a), the CTR simulation suffers from two weak an AABW circulation ($\sim$2.5 Sv) limited northward to 10°N. Consequently, NADW invades the deepest part of the North Atlantic. By contrast in the DWS experiment (Fig. 7b), the inflow of AABW is stronger ($>$4 Sv) and penetrates northward to 40°N, in good agreement with observations (Mantyla and Reid, 1983; Schmitz and McCartney, 1993). As a result, the NADW circulation becomes shallower ($<$3.5 km), and slightly weaker since it exports 16.8 Sv at 30°S (close to derived observation estimates (Schlitzer, 1993)) compared to 18.3 Sv in the CTR simulation. But except for these changes, the circulation pattern is identical: NADW forms in the GIN seas (8 Sv), joins the Deep North Atlantic through the Denmark Strait where it incorporates, south of Greenland, an additional supply of less dense water and finally flows across the Atlantic toward the South.

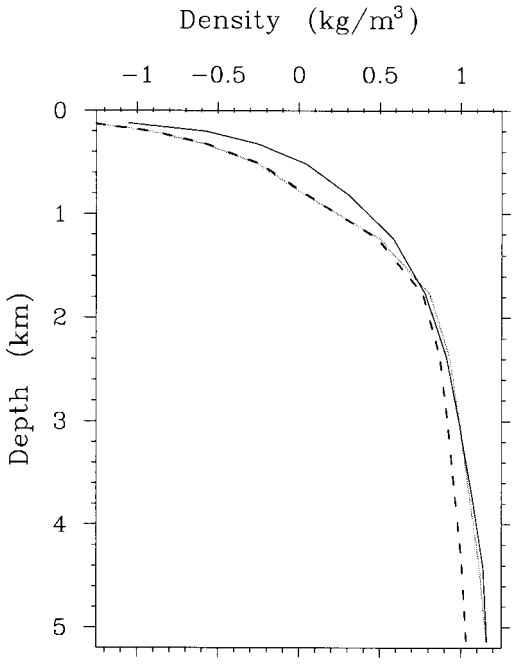


*Fig. 5.* Global mean vertical profile of density (kg/m$^3$) relative to a reference water mass (4°C, 34 psu), for experiment DWS (light solid line) compared to experiment CTR (doted line) and Levitus (1982) data (thick solid line).

The Denmark Strait overflow is better represented with the downsloping parameterization since dense water can thus easily follow the bottom. But this has no major effect on the large scale circulation. This is mainly due to the fact that the increase in AABW density tends to dominate the thermohaline circulation changes. Secondly, for the Denmark Strait Outflow, the "original" large scale circulation is directed southward, with and without the parameterization. Here the downsloping flow tends simply to replace the two steps mechanism, horizontal advection of dense DSOW followed by deep convective adjustments. A diagnostic (not shown) of the gravitational energy released by convective adjustments confirms this interpretation.

Concerning the Mediterranean Sea, the control experiment suffers from an overestimation of the outflow (2.2 Sv) due to the unrealisticly large width of the Gibraltar Strait, since, on a "B grid", 2 grid boxes ($\simeq$600 km) are necessary to allow an exchange through one velocity point. The downsloping parameterization induces here a strong mixing that limits the geostrophic flow across the strait, leading to a more realistic outflow (1.6 Sv, compared to observations around 1. Sv). However we suspect this enhanced mixing mechanism not to be physically justified. It appears that, the detailed effect of the parameterization cannot be properly discussed as long as the strait width is not reduced. This reduction of the Mediterranean water outflow cools and freshens the North Atlantic Intermediate Water, as showed on Fig. 8.

With the downsloping parameterization, despite the increase of AABW northward flow at 50°S (from 9.0 Sv to 10.9 Sv), the antarctic meridional circulation cell (counter-clockwise), associated with a downwelling near the continent, is reduced by 2 Sv (from 26 Sv to 24 Sv). The reason thereof is that the dense shelf water can directly reach the deep ocean and does not contribute to the large scale dynamic explicitly resolved in the model, i.e., in this case, the downwelling near Antarctica. Thus, we can expect a different ventilation scheme of the Deep Southern Ocean with a larger direct contribution of shelf water and, on the contrary, a reduction of the open ocean surface water supply, since the Antarctic meridional cell is weaker and the stronger deep ocean stratification is prone to reduce vertical mixing and open ocean deep convection. This aspect has to be confirmed with additional passive tracers experiments.

The zonally averaged salinity difference (DWS–CTR) (Fig. 8a,b) illustrates the water mass properties changes. The salinity on Antarctic shelves is strongly reduced, due to larger exchange with the open ocean. For the same reason, the deep Southern Ocean (south of 50°S) becomes saltier ($>+0.05$ psu), slightly colder ($-0.2$ to $-0.3$°C, Fig. 6b) and then denser (Fig. 6a), from $+0.02$ kg/m$^3$ at 500 m depth to $+0.12$ kg/m$^3$ at the bottom. In the Atlantic, the decrease in the circulation of NADW, more saline and warmer than AABW, dominates both temperature and salinity changes and is responsible for a cooling (larger than 0.5°C) and freshening ($-0.05$ psu, Fig. 8a). In the other basins, the increase of AABW salinity balances the reduction of the salty NADW outflow, totally in the Pacific (Fig. 8b) and only partially in the Indian Ocean, whereas for the temperature changes, those two tendencies work together and impose a cooling of 0.5°C (Fig. 6b).

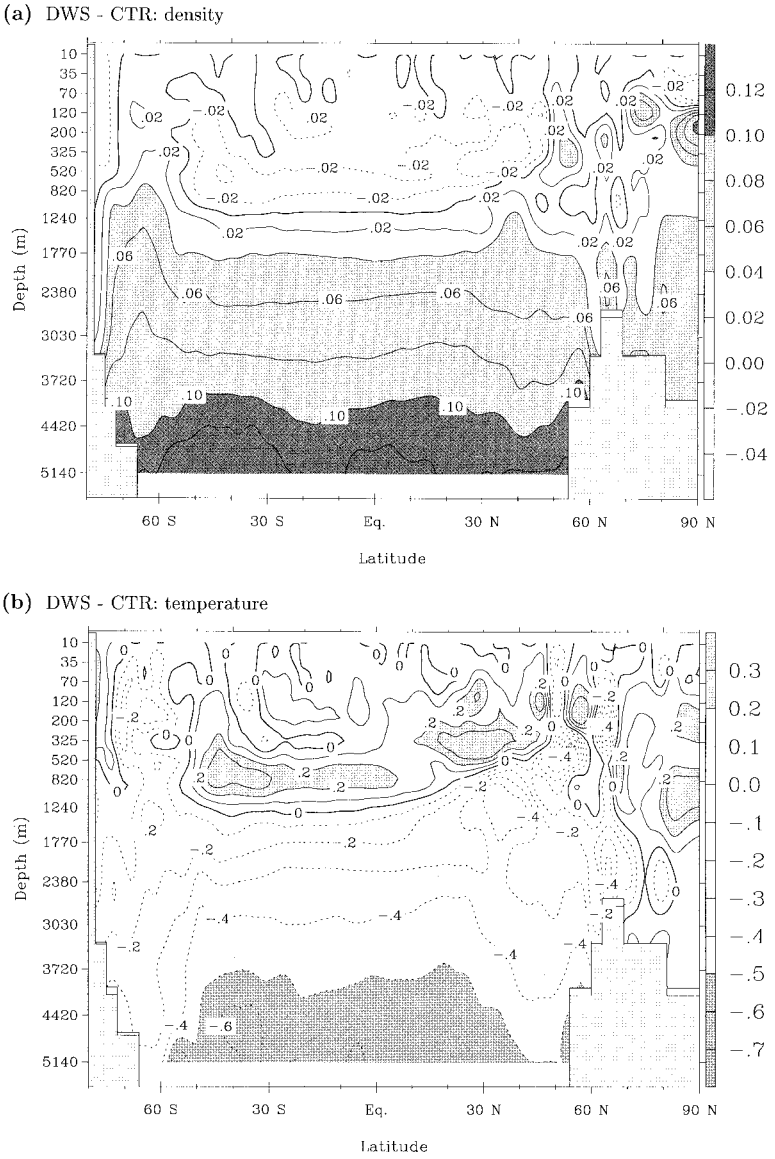


*Fig. 6.* Global zonal mean differences between the two experiments with and without the parameterization (DWS–CTR): (a) density (kg/m$^3$) and (b) temperature (°C).

## 5. Conclusion

A parameterization of downsloping flow, designed for coarse resolution model, has been established and incorporated in the UCL–OGCM. This parameterization enables dense water exchange from the top of a bathymetric step with the neighbouring deeper column. The downsloping flow ignores the large scale geostrophic constraint and is only function of the horizontal density difference at the shelf edge, through a simple linear relation. Two equilibrium experiments under annual mean climatological forcing, with and without the parameterization, reveal its

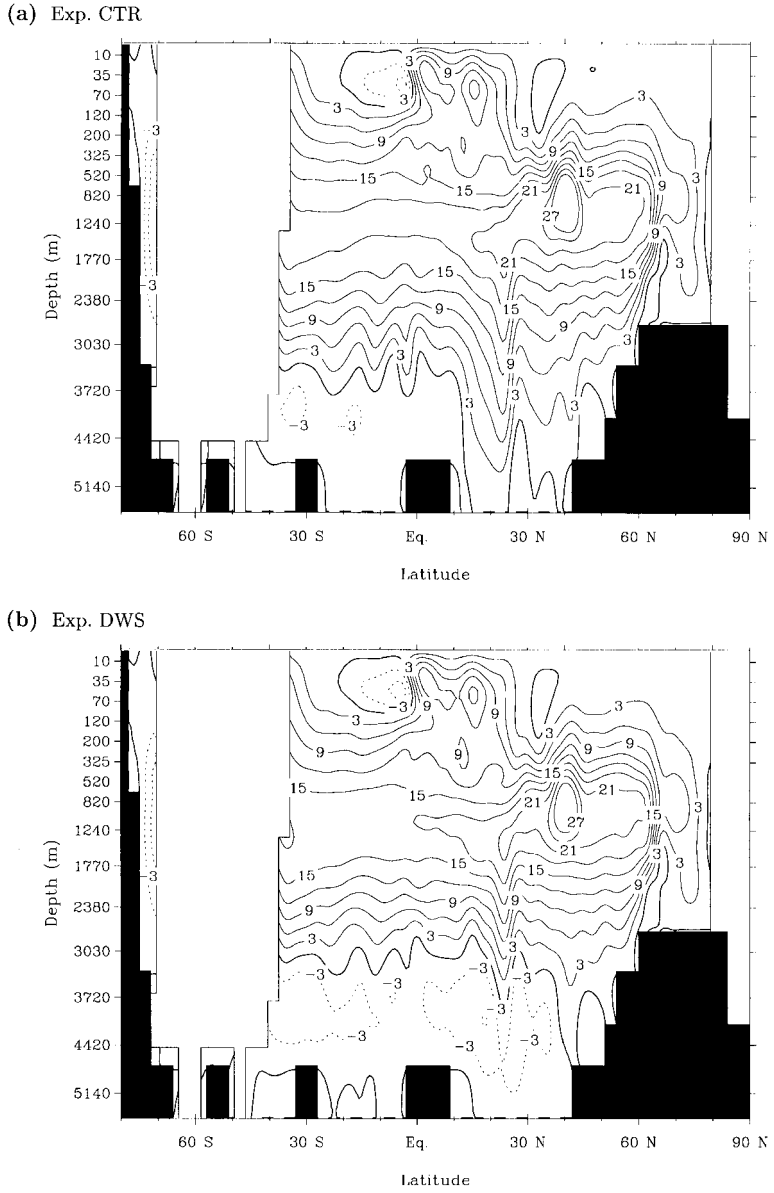


*Fig. 7.* Meridional transport stream function (Sv) for the Atlantic ocean. Circulation is clockwise around a maximum and is shown for (a) experiment CTR and (b) experiment DWS. The contour interval is 3 Sv.

main effects. Firstly, it increases the exchange between the shelf and the open ocean, the first being too isolated in the control experiment. Secondly, this parameterization improves the density structure of the deep ocean and gives a better representation of AABW density and circulation. Also expected, the ventilation pattern of the deep southern ocean could be modified, with a different distribution between shelf water and open ocean surface water contributions. This effect needs further investigations.

Furthermore, the sensitivity experiment tends

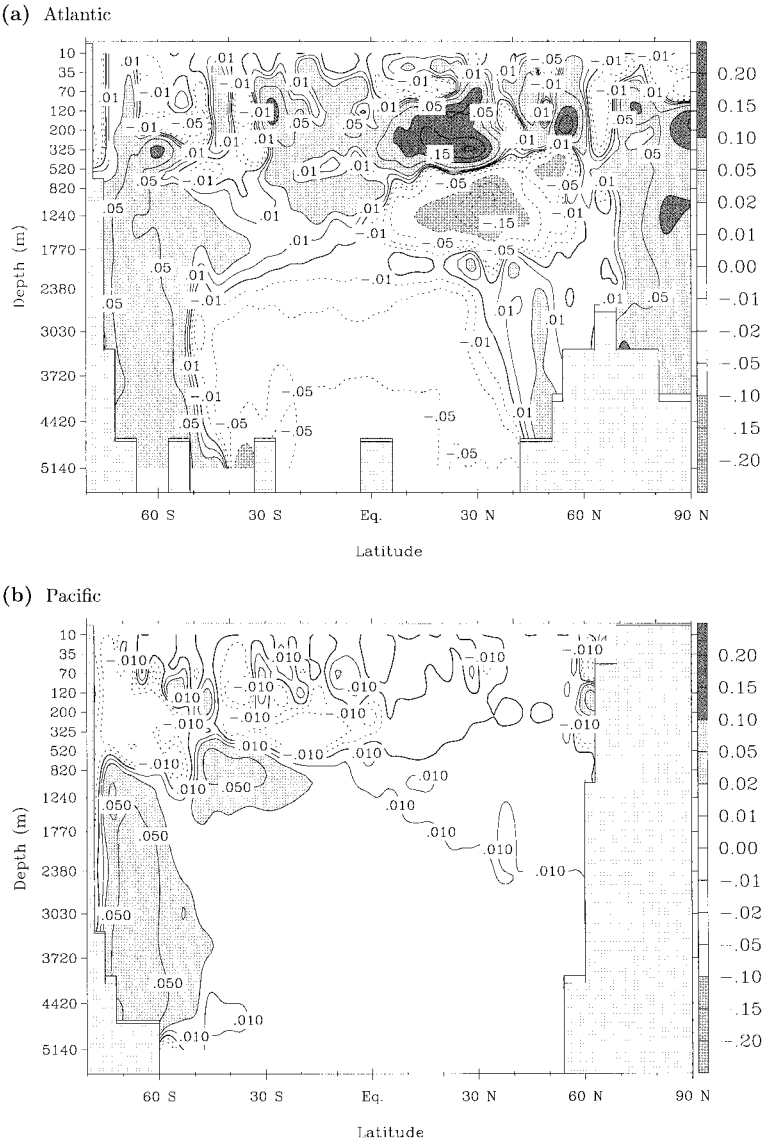


*Fig. 8.* Zonal mean salinity differences (psu) between the two experiments with and without the parameterization (DWS–CTR) for (a) the Atlantic and (b) the Pacific.

to prove that the small scale downsloping process, that is not represented in most OGCMs, has a significant impact on the model results. This completes the explanation to the question risen by Toggweiler and Samuels (1995) concerning the unrealistically high salinity adjustment needed to give better deep ocean properties. In our case, a moderate salt enhancement limited to Antarctic continental shelves, that lies within the range of observations (Zwally et al., 1985), is sufficient to increase the deep ocean density, provided the downsloping parameterization is used.

This parameterization could be improved using a space-dependent coefficient of proportionality $\gamma$, according to the local small scale bottom shape. But practically, this topography regional depend-

ency seems difficult to establish for the whole ocean. This test suggests that $\gamma = 10$ s lies in the upper range of the possible values (e.g., the downsloping flow are somewhat over-estimated), but does not give rise to spurious effects. This strengthens the confidence in the parameterization that we gain from this validation test. The only exception to this general rule is the Gibraltar Strait where the downsloping parameterization, through indirect interaction with the poorly resolved dynamic inside the Strait, weakens the exchange between Mediterranean and Atlantic Ocean. In this case, the coefficient $\gamma$ is most likely too large, because it is associated with a section of the Strait more than 60 times wider than the real one. But, even there, the reduction of the Mediterranean outflow induced by the parameterization could appear realistic.

Recently new parameterizations based on an explicit representation of the bottom boundary layer have been proposed. This parameterization is certainly not so accurate and much more simple. However, because of its simplicity and its low cost in terms of computer time, this new parameterization represents a valuable first approach for long term integration since it reveals only positive effects. Contrary to bottom layer schemes, this parameterization allows a downsloping flow to enter an intermediate level, different from the bottom level. This is an advantage since in coarse horizontal resolution models, steep bottom slopes are often represented by a wall of several vertical levels height, and real downsloping flows are not always enough dense to reach the bottom.

Note that the annual mean restoring forcing used for this sensitivity experiment is not the most realistic one. However this simple and widely used forcing provides a first idea of this parameterization effect and allows a comparison with previous studies (Toggweiler and Samuels, 1995). The ocean–sea ice coupled model "CLIO" (Goosse et al., 1997a,b) is currently testing this parameterization using a full seasonal forcing based on climatological fluxes. The preliminary results seem promising and confirm the main tendency presented here. Specially, the improvement of the AABW properties and of the exchanges between Antarctic shelf and open ocean remain the dominant effects of the parameterization even though the AABW circulation was reasonably well reproduced in the experiment without the downsloping flow parameterization (Goosse et al., 1997a).

## 6. Acknowledgements

We warmly thank E. Deleersnijder for encouragement and helpful comments on various aspects of this study. P. P. Mathieu and P. Tulkens helped to improve the clarity of the manuscript. We also thank an anonymous referee for his positive remarks. H. Goosse is Senior Research Assistant with the National Fund for Scientific Research (Belgium) and J. M. Campin is supported by the European Union (Contract ENV4-CT95-0131). This work was done within the scope of the Global Change and Sustainable Development Programme (Belgian State, Prime Minister's Services, Federal Office for Scientific, Technical and Cultural Affairs, Contract CG/DD/09A) and the Concerted Research Action 097/02-208 (French Community of Belgium, Department of Education, Research and Formation).

## 7. Appendix

*Model description*

The model used in this study is based on primitives equations, and relies on the commonly used hydrostatic and Boussinesq approximations. The governing equations will be briefly presented here.

The conservation of mass (4) and scalar quantities $s$ (potential temperature $\theta$ (°C), salinity $S$ (psu) or any additional tracer) (5), and momentum equation in the horizontal plane (6) and in the vertical direction (7) read:

$$\frac{\partial w}{\partial z} + \nabla \cdot \bar{u} = 0, \tag{4}$$

$$\frac{\partial s}{\partial t} + \bar{u} \cdot \nabla s + w \frac{\partial s}{\partial z} = A_h \nabla^2 s + \frac{\partial}{\partial z}\left( A_z \frac{\partial s}{\partial z} \right), \tag{5}$$

$$\frac{\partial \bar{u}}{\partial t} + (\bar{u} \cdot \nabla)\bar{u} + w \frac{\partial \bar{u}}{\partial z} + \bar{f} \times \bar{u} = -\frac{1}{\rho_0} \nabla p + \nu_h \nabla^2 \bar{u} + \frac{\partial}{\partial z}\left( \nu_z \frac{\partial \bar{u}}{\partial z} \right), \tag{6}$$

$$p(z) = \rho_0 g \eta + \int_z^0 \rho(\theta, S, \zeta) g \, \mathrm{d}\zeta, \tag{7}$$

with density $\rho$ given by the non linear equation of state (Eckart, 1958):

$$\rho = \rho(\theta, S, z), \tag{8}$$

where $x$, $y$, $z$ and $\bar{e}_x, \bar{e}_y, \bar{e}_z$ are the 3 coordinates (increasing eastward, northward and upward) and associated local base vectors;

$$\bar{v} = \bar{u} + w\bar{e}_z = u\bar{e}_x + v\bar{e}_y + w\bar{e}_x$$

is the velocity; $t$, $\lambda$, $\phi$, $\eta$ and $p$ are the time, longitude, latitude, sea surface elevation and pressure; $\bar{g} = -g\bar{e}_z$ is the gravity, $\Omega$ and $\bar{f} = 2\Omega \sin(\phi)\bar{e}_z$ are the earth rotation and Coriolis factor; $A$, is the diffusivity ($m^2/s$) and $\nu$, is the viscosity ($m^2/s$). The full expression of horizontal space differencing operators $\nabla(\ )$, $\nabla\cdot(\ )$, $\nabla^2(\ )$ in a general orthogonal coordinate system includes metric coefficients (Deleersnijder et al., 1997) but, for simplicity, the compressed form is retained here.

With the free surface formulation, the sea surface elevation $\eta$ becomes a prognostic variable and is governed by the barotropic subset equations, obtained after vertical integration from the bottom ($z = -H$) to the surface ($z \simeq 0$), of the eqs. (4) and (6):

$$\frac{\partial \eta}{\partial t} = w_{z=0} = -\nabla \cdot \bar{U}, \tag{9}$$

$$\frac{\partial}{\partial t}\bar{U} + \bar{f} \times \bar{U} = -gH\nabla\eta + \nu_h \nabla^2 \bar{U} + \bar{\mathscr{F}}_U, \tag{10}$$

where $\bar{U} = \int_{-H}^{0} \bar{u}\, dz$ and $\bar{\mathscr{F}}_U$ integrates all the remaining terms of eq. (6) not resolved explicitly in (10) (Deleersnijder and Campin, 1995).

The outline of the numerical discretization used in our model will be presented here and more details can be found in Campin (1997). The spatial discretization, is achieved on the Arakawa "*B* grid" using the "*z*-coordinate" for the vertical direction, similar to the one described by Bryan (1969). As opposed to the leapfrog time stepping of the GFDL model (Bryan, 1969), our model uses the explicit Euler forward-backward time stepping for both barotropic eqs. (9, 10) and baroclinic eqs. (5, 6). The vertical terms are computed implicitly and the Coriolis terms are solved semi-implicitly. As described by Deleersnijder and Campin (1995), the mode splitting technique proposed by Killworth et al. (1991) is used to solve separately the barotropic subset eqs. (9, 10) with a small time step, whereas the baroclinic variables are integrated with a longer one.

The convergence accelerator of Bryan and Lewis (1979) has been implemented in order to save computer time, leading to shorter time step ($\Delta t_u =$ 3 h) for baroclinic velocity ($u$, $v$) than scalar quantities. The scalar time step is also longer below 500 m, from $\Delta t_s = 30$ h at the surface up to 96 h, in the deeper level. During one model iteration, 26 sub-iterations ($\Delta t_b = 5$ min) are performed to compute the updated barotropic variables ($\eta$, $\bar{U}$) that are averaged over the 26 values. This results in an additional acceleration factor between baroclinic and barotropic variables, advanced in time to 3 h, and $5 \times 26/2 = 65$ min, respectively.

The simple centered in space advection scheme is used for eq. (6) and remains stable thanks to a large — but common for low resolution OGCM — horizontal viscosity ($\nu_h = 10^5$ $m^2/s$) required to represent western boundary currents. For the advection of scalar quantities, the fractional time stepping (Yanenko, 1971) combined with Lax–Wendroff advection scheme guarantees the numerical stability. Furthermore, a moderate horizontal diffusion ($A_h = 300$ $m^2/s$) and an hybrid upwind/Lax–Wendroff advection scheme (Campin, 1997) derived from James (1986) limit the occurrence and growth of spurious local extrema.

The vertical diffusivity and viscosity in the upper 500 m are computed using Pacanowski and Philander (1981) parameterization with a background vertical diffusivity increasing with depth, following the profile proposed by Bryan and Lewis (1979). A convective adjustment removes gravitational instabilities wherever the water column is unstable.

In order to avoid the North Pole singularity associated with geographical coordinates, the model grid is composed of two spherical sub-grids (Deleersnijder et al., 1997): One sub-grid has its poles located on the Equator and covers the Arctic and the North Atlantic; the second is the usual longitude and latitude grid and covers the remaining part of the ocean. The two grids are connected at the Equator, in the Atlantic. The model resolution is $3^\circ \times 3^\circ$ and has 15 irregularly spaced vertical levels, from 20 m thickness at the surface to more than 700 m at 5000 m depth. Because the two spherical sub-grids cannot explicitly resolve the Bearing Strait, the flow through this Strait is computed using a parameterization based on the geostrophic control theory (Goosse et al., 1997b). The model bathymetry is derived

from ETOPO 5 (1986), according to the criterion that grid boxes containing more than 40% of water are oceanic. Due to the low resolution of the model, the narrow passages have been widen up to allow exchange of water (Gibraltar Strait, Hudson Strait, Indonesian passage, Japan Sea ...). A deepening of the Greenland Iceland Scotland straits (model depth: $H_{\text{sill}} = 1400$ m) allows a better representation of the exchange between the GIN Seas and the North Atlantic, as also done in some other $z$-coordinate OGCMs (Toggweiler et al., 1989; Manabe et al., 1991; Maier-Reimer et al., 1993; Roberts et al., 1996).

## REFERENCES


Aagaard, K., Swift, J. H. and Carmack, E. C. 1985. Thermohaline circulation in the Arctic Mediterranean Seas. *J. Geophys. Res.* **90**, 4833–4846.

Baines, P. G. and Condie, S. 1998. Observations and modelling of Antarctic downslope flows: a review. In: *Ocean, ice and atmosphere interactions at the Antarctic continental margin* (eds. S. S. Jacobs and R. F. Weiss). *Antarctic Research Series* **75**, American Geophysical Union, Washington DC, 29–49.

Beckmann, A. and Döscher, R. 1997. A method for improved representation of dense water spreading over topography in geopotential-coordinate models. *J. Phys. Oceanogr.* **27**, 581–591.

Bryan, K. 1969. A numerical method for the study of the circulation of the world ocean. *J. Comp. Phys.* **4**, 347–376.

Bryan, K. and Lewis, L. J. 1979. A water mass model of the world ocean. *J. Geophys. Res.* **84**, 2503–2517.

Cai, W. and Baines, P. G. 1996. Interactions between thermohaline- and wind-driven circulations and their relevance to the dynamics of the Antarctic Circumpolar Current, in a coarse-resolution global ocean general circulation model. *J. Geophys. Res.* **101**, 14,073–14,093.

Campin, J.-M. 1997. *Modélisation tridimensionnelle de la circulation générale océanique lors du dernier maximum glaciaire*. PhD thèse, Université Catholique de Louvain, 342 pp.

Cavalieri, D. J. and Martin, S. 1994. The contribution of Alaskan, Siberian, and Canadian coastal polynyas to the cold halocline layer of the Arctic Ocean. *J. Geophys. Res.* **99**, 18,343–18,362.

Chapman, D. C. and Gawarkiewicz, G. 1995. Offshore transport of dense shelf water in the presence of a submarine canyon. *J. Geophys. Res.* **100**, 13,373–13,387.

Da Silva, A. M., Young, C. C. and Levitus, S. 1994. *Atlas of surface marine data 1994*, vol. 1. *Algorithms and procedures*. NOAA Atlas NESDIS 6, US Govt. Printing Office, Washington DC, 83 pp.

Deleersnijder, E. and Campin, J.-M. 1995. On the computation of the barotropic mode of a free-surface world ocean model. *Ann. Geophysicae* **13**, 675–688.

Deleersnijder, E., Beckers, J.-M., Campin, J.-M., El Mohajir, M., Fichefet, T. and Luyten, P. 1997. Some mathematical problems associated with the development and use of marine models. In: *The mathematics of models for climatology and environment* (ed. J. Ildefonso Diax). Springer-Verlag, Berlin Heidelberg, 39–86.

Dickson, R. R. and Brown, J. 1994. The production of North Atlantic Deep Water: sources, rates, and pathways. *J. Geophys. Res.* **99**, 12,319–12,341.

Eckart, C. 1958. Properties of water, Part II: The equation of state of water and sea water at low temperatures and pressures. *Am. J. Sci.* **256**, 225–240.

England, M. H. 1993. Representing the global-scale water masses in ocean general circulation models. *J. Phys. Oceanogr.* **23**, 1523–1552.

ETOPO 5 1986. *Global 5′ × 5′ depth and elevation*. Available from National Geophysical Data Center, NOAA, US Dept of Commerce, Code E/GC3, Boulder, CO 80303.

Fahrbach, E., Peterson, R. G., Rohardt, G., Schlosser, P. and Bayer, R. 1994. Supression of bottom water formation in the southeastern Weddell Sea. *Deep-Sea Res.* **41**, 389–411.

Foldvik, A., Gammelsroed, T. and Toerresen, T. 1985. Circulation and water masses on the southern Weddell Sea shelf. In: *Oceanography of the Antarctic continental shelf* (ed. S. S. Jacobs). *Antarctic Research Series* **43**, American Geophysical Union, Washington DC, 5–20.

Foster, T. D. and Carmack, E. C. 1976. Frontal zone mixing and Antarctic bottom water formation in the southern Weddell Sea. *Deep-Sea Res.* **23**, 301–317.

Gallée, H. 1995. Simulation of the mesocyclonic activity in the Ross Sea, Antarctica. *Mon. Wea. Rev.* **123**, 2051–2069.

Gill, A. E. 1973. Circulation and bottom water production in the Weddell Sea. *Deep-Sea Res.* **20**, 111–140.

Gnanadesikan, A., Pacanowski, R. C. and Winton, M. 1998. Representing the bottom boundary layer in the GFDL ocean model: model framework, dynamical impacts, and parameter sensitivity. *J. Phys. Oceanogr.*, in press.

Goosse, H., Campin, J.-M., Fichefet, T. and Deleersnijder, E. 1997a. The impact of sea-ice formation on the properties of Antarctic bottom water. *Ann. Glaciology* **25**, 276–281.

Goosse, H., Campin, J.-M., Fichefet, T. and Deleersnijder, E. 1997b. Sensitivity of a global ice–ocean model to the Bering Strait throughflow. *Clim. Dyn.* **13**, 349–358.

Goosse, H., Fichefet, T. and Campin, J.-M. 1997c. The effects of the water flow through the Canadian Archi-

pelago in a global ice–ocean model. *Geophys. Res. Lett*. **24**, 1507–1510.

Gordon, A. L., Huber, B. A., Hellmer, H. H. and Ffield, A. 1993. Deep and bottom water of the Weddell Sea's western rim. *Science* **262**, 95–97.

Han, Y.-J. and Lee, S.-W. 1983. An analysis of monthly mean wind stress over the global ocean. *Mon. Wea. Rev*. **111**, 1554–1566.

Haney, R. L. 1991. On the pressure gradient force over steep topography in sigma coordinate ocean models. *J. Phys. Oceanogr*. **21**, 610–619.

Harvey, L. D. D. 1996. Polar boundary layer plumes and bottom water formation: a missing element in ocean general circulation models. *J. Geophys. Res*. **101**, 20,799–20,808.

Hirst, A. C. and Cai, W. 1994. Sensitivity of a world ocean GCM to changes in subsurface mixing parameterization. *J. Phys. Oceanogr*. **24**, 1256–1279.

Jacobs, S. S., Amos, A. F. and Bruchhausen, P. M. 1970. Ross Sea oceanography and Antarctic bottom water formation. *Deep-Sea Res*. **17**, 935–962.

James, I. D. 1986. A front-resolving sigma coordinate sea model with a simple hybrid advection scheme. *Appl. Math. Modelling* **10**, 87–92.

Jungclaus, J. H., Backhaus, J. O. and Fohrmann, H. 1995. Outflow of dense water from the Storfjord in Svalbard: a numerical model study. *J. Geophys. Res*. **100**, 24,719–24,728.

Killworth, P. D. 1977. Mixing on the Weddell Sea continental slope. *Deep-Sea Res*. **24**, 427–448.

Killworth, P. D. 1983. Deep convection in the world ocean. *Rev. Geophys*. **21**, 1–26.

Killworth, P. D. and Edwards, N. R. 1998. A turbulent bottom boundary layer code for use in numerical ocean models. *J. Phys. Oceanogr*., in press.

Killworth, P. D., Stainforth, D., Webb, D. J. and Paterson, S. M. 1991. The development of a free surface Bryan–Cox–Semtner model. *J. Phys. Oceanogr*. **21**, 1333–1348.

Levitus, S. 1982. *Climatological atlas of the world ocean*. NOAA Prof. pap. 13, US Govt. Printing Office, Washington DC, 173 pp.

Maier-Reimer, E., Mikolajewicz, U. and Hasselmann, K. 1993. Mean circulation of the Hamburg LSG OGCM and its sensitivity to the thermohaline surface forcing. *J. Phys. Oceanogr*. **23**, 731–757.

Manabe, S., Stouffer, R. J., Spelman, M. J. and Bryan, K. 1991. Transient responses of a coupled ocean–atmosphere model to gradual changes of atmospheric $CO_2$. Part I: Annual mean response. *J. Climate* **4**, 785–818.

Mantyla, A. W. and Reid, J. L. 1983. Abyssal characteristics of the World Ocean waters. *Deep-Sea Res*. **30**, 805–833.

Muench, R. D. and Gordon, A. L. 1995. Circulation and transport of water along the western Weddell Sea margin. *J. Geophys. Res*. **100**, 18,503–18,515.

Pacanowski, R. C. and Philander, S. G. H. 1981. Parameterization of vertical mixing in numerical models of tropical oceans. *J. Phys. Oceanogr*. **11**, 1443–1451.

Polzin, K. L., Speer, K. G., Toole, J. M. and Schmitt, R. W. 1996. Intense mixing of Antarctic bottom water in the equatorial Atlantic Ocean. *Nature* **380**, 54–57.

Price, J. F. and O'Neil Baringer, M. 1994. Outflows and deep water production by marginal seas. *Prog. Oceanogr*. **33**, 161–200.

Price, J. F., O'Neil Baringer, M., Lueck, R. G., Johnson, G. C., Ambar, I., Parrilla, G., Cantos, A., Kennelly, M. A. and Sanford, T. B. 1993. Mediterranean outflow mixing and dynamics. *Science* **259**, 1277–1282.

Roberts, M. J., Marsh, R., New, A. L. and Wood, R. A. 1996. An intercomparison of a Bryan–Cox-type ocean model and an isopycnic ocean model. Part I: The subpolar gyre and high-latitude processes. *J. Phys. Oceanogr*. **26**, 1495–1527.

Schauer, U. 1995. The release of brine-enriched shelf water from Storfjord into the Norwegian Sea. *J. Geophys. Res*. **100**, 16,015–16,028.

Schauer, U., Muench, R. D., Rudels, B. and Timokhov, L. 1997. Impact of eastern Arctic shelf waters on the Nansen Basin intermediate layers. *J. Geophys. Res*. **102**, 3371–3382.

Schlitzer, R. 1993. Determining the mean, large-scale circulation of the Atlantic with the adjoint method. *J. Phys. Oceanogr*. **23**, 1935–1952.

Schmitz, W. J. and McCartney, M. S. 1993. On the North Atlantic circulation. *Rev. Geophys*. **31**, 29–49.

Shapiro, G. I. and Hill, A. E. 1997. Dynamics of dense water cascades at the shelf edge. *J. Phys. Oceanogr*. **27**, 2381–2394.

Smith, P. C. 1975. A streamtube model for bottom boundary currents in the ocean. *Deep-Sea Res*. **22**, 853–873.

Steele, M., Morison, J. H. and Curtin, T. B. 1995. Halocline water formation in the Barents Sea. *J. Geophys. Res*. **100**, 881–894.

Swift, J. H., Takahashi, T. and Livingston, H. D. 1983. The contribution of the Greenland and Barents Seas to the deep water of the Arctic Ocean. *J. Geophys. Res*. **88**, 5981–5986.

Toggweiler, J. R. and Samuels, B. 1995. Effect of sea ice on the salinity of Antarctic bottom waters. *J. Phys. Oceanogr*. **25**, 1980–1997.

Toggweiler, J. R., Dixon, K. and Bryan, K. 1989. Simulations of radiocarbon in a coarse-resolution word ocean model (1). Steady state prebomb distributions. *J. Geophys. Res*. **94**, 8217–8242.

Yanenko, N. N. 1971. *The method of fractional steps*. Springer-Verlag, New York, 160 pp.

Zwally, H. J., Comiso, J. C. and Gordon, A. L. 1985. Antarctic offshore leads and polynyas and oceanographic effects. In: *Oceanography of the Antarctic continental shelf* (ed. S. S. Jacobs). *Antarctic Research Series* **43**, American Geophysical Union, Washington DC, 203–226.